

SHARP-QoS: Sparsely-gated Hierarchical Adaptive Routing for joint Prediction of QoS

Suraj Kumar, *Student Member, IEEE*, Arvind Kumar, Soumi Chattopadhyay, *Senior Member, IEEE*

Abstract—Dependable service-oriented computing relies on multiple Quality-of-Service (QoS) parameters that are essential to measure service optimality. However, real-world QoS data are extremely sparse, noisy, and shaped by hierarchical dependencies arising from QoS interactions, geographical constraints, and network-level factors, making accurate QoS prediction challenging. Existing deep learning-based methods often predict each QoS parameter separately, requiring multiple similar models, which increases computational overhead and leads to poor generalization. Although recent joint QoS prediction studies have explored shared architectures, they suffer from negative transfer due to loss-scaling issues caused by inconsistent numerical ranges across QoS parameters and further struggle with inadequate representation learning and suboptimal joint optimization, resulting in degraded accuracy. In this paper, we present a data-driven strategy for joint QoS prediction, called SHARP-QoS, that addresses these limitations through three complementary components. First, we introduce a dual mechanism to extract the hierarchical features from both QoS and contextual structures using hyperbolic convolution formulated in the Poincaré ball. Second, we propose an adaptive feature-sharing mechanism that allows feature exchange across informative QoS and contextual signals. A gated feature fusion module is introduced to support dynamic feature selection among structural and shared representations. Third, we design an EMA-based loss balancing strategy that enables stable joint QoS-optimization, thereby mitigating the negative transfer. Evaluations on three datasets with two, three, and four QoS parameters demonstrate that our framework outperforms both single- and multi-task baselines. Extensive study on the module, and hyperparameters sensitivity shows that our model effectively addresses major challenges, including sparsity resilience, robustness to outliers, and strong cold-start handling, while maintaining moderate computational overhead, underscoring its capability for reliable joint QoS prediction.

Index Terms—Joint QoS Prediction, Service Recommendation, Multi-task Learning, Graph Convolution Networks, Hyperbolic Space

I. INTRODUCTION

Service-oriented architectures (SoA) utilize independent, reusable, and loosely coupled services to build web/cloud applications [1], [2]. However, with the rapid advancement of networking/cloud-based AI technologies, numerous service providers offer functionally similar services, making it increasingly difficult for users or businesses to select the optimal service. Existing studies show that a service's non-functional parameters (e.g. response time, throughput, and reliability),

Suraj Kumar and Soumi Chattopadhyay are with the Dept. of CSE, Indian Institute of Technology Indore, India 453552. (email: {phd2301101002, soumi}@iiti.ac.in). Corresponding author: Soumi Chattopadhyay. This work has been submitted to the IEEE for possible publication. Copyright may be transferred without notice, after which this version may no longer be accessible.

collectively known as Quality of Service (QoS) parameters, can be effectively used to assess both service optimality and runtime performance. Thus, QoS parameters have been widely utilized for the service selection, composition, and recommendation. Nevertheless, in real-world service ecosystems, obtaining QoS values for all available services is a non-trivial task, leading to high resource and time consumption when monitored manually. Hence, QoS prediction has emerged as a challenging task, often resembling the problem of missing value prediction [3], [4], [5].

Traditional QoS prediction methods primarily rely on collaborative filtering (CF), often using user/service similarity [6], [7], [3]. However, they continue to struggle with data sparsity, cold-start cases, and outliers. To address these challenges, reconstruction-based predictive models have emerged. These include matrix factorization (MF) [8], [4], exploiting first-order (linear) features, factorization machines (FM) [9] extend this to second-order interactions, and deep architectures (e.g. multilayer perceptrons (MLP) [5], [10] and graph convolutional networks (GCNs)), capture nonlinear, higher-order features/graph structure [11], [12]. Hybrid methods, combining these approaches, further enhance QoS prediction performance [13], [5], [14]. While effective, these methods struggle when multiple QoS parameters must be jointly considered for optimal service performance. For instance, the ideal functioning of autonomous vehicles (AVs) relies on precise decision-making based on multiple QoS parameters that dictate service performance. However, designing separate models for each QoS parameter leads to increased computational costs (e.g., more parameters and floating-point operations), poor generalization, and longer inference times. Hence, there is a need for a unified framework that enables joint QoS modeling, allowing the simultaneous prediction of all QoS parameters [15], [16].

First proposed by [17], multi-task learning (MTL) enables simultaneous prediction across multiple tasks by sharing knowledge, improving generalization, and capturing task interdependencies. However, MTL for QoS prediction is challenging due to several underlying issues, including data sparsity, cold start, and outliers, which essentially require attentive multi-task representation learning. Recent studies have formulated MTL approaches for QoS prediction. DNM [15] introduced additive and multiplicative cross-context interactions, followed by an MLP to capture higher-order dependencies. JQSP [18] employed a graph attention network (GAT) to ID-based features and used an outlier-sensitive loss. MGEN [19] utilized a gated expert network to capture context-specific and QoS-specific latent features. HTG [20] adopted a GAT for cold-start-aware MTL but heavily relies on sensitive topology

information. Although competitive, they often encounter a task dominance problem during training due to the numerical range difference of QoS parameters, leading to negative transfer. To address this issue, PMT [16] optimized task losses using a Gaussian likelihood with homoscedastic uncertainty via a multi-expert architecture with an attention mechanism. Besides this, WAMTL [21] adopted dynamic weight averaging (DWA) to adjust loss weights based on past loss reduction rates, and used a multi-gate mixture-of-experts (MoE) framework. However, this approach suffers from overfitting due to the over- or under-utilization of experts.

Despite these advances, existing methods still overlook implicit hierarchical dependencies and shared contextual correlations across QoS parameters. Moreover, task-balancing strategies used in works such as [21], [16] often exhibit numerical instability and oscillatory convergence, resulting in suboptimal multi-task performance. To address these limitations, we propose a unified framework for joint QoS prediction, called SHARP-QoS, which allows adaptive multi-task representation learning by leveraging contextual data and complementary QoS signals. The framework comprises three key components: (i) We introduce a Hierarchical Feature Extraction Block (HFEB) to capture implicit hierarchical dependencies across QoS and contextual features, enabling richer representations while preserving user/service privacy. (ii) Inspired by Sub-Network Routing (SNR) [22], a dual feature exchange mechanism is designed to share across both QoS- and contextual-features, while maintaining computational efficiency, unlike previous approaches. Besides this, a gated feature fusion module is employed, which selectively integrates relevant representations from shared and structure-aware features. (iii) The Exponential Moving Average (EMA) is introduced to smooth short-term fluctuations in training due to loss scale, ensuring robust optimization for joint QoS prediction.

The key **contributions** are summarized below:

- We propose a data-driven joint QoS prediction framework that leverages implicit hierarchical features from both QoS and context data. A feature-sharing and fusion layer is introduced that enables effective parameter sharing through QoS and contextual features, and dynamically selects task-specific features among structural and shared representations, resulting in enhanced QoS prediction performance.
- We introduce an EMA-based loss balancing strategy that reduces short-term oscillation and resolves inter-attribute conflicts across multiple QoS tasks, mitigating the negative transfer problem caused by numerical range discrepancies among QoS parameters, leading to faster convergence and improved generalization across tasks.
- Extensive experiments are conducted on three datasets: WS-DREAM-2T [23], small-3T [16], and a gRPC-4T dataset [14], covering two, three, and four QoS parameters, respectively. To ensure the reliability of our results, we include ablation studies, hyperparameter analysis, impact of outliers and cold-start, and statistical significance tests, demonstrating the effectiveness of our method.

II. PRELIMINARIES

Hyperbolic geometry has emerged as a powerful tool for modeling hierarchical and scale-free structures due to its constant negative curvature and exponential expansion [24]. In contrast to Euclidean space (zero curvature), hyperbolic space represents hierarchies and heavy-tailed degree distributions with lower distortion [25]. We adopt the Poincaré ball model to perform graph convolution in hyperbolic space, as it provides a conformal manifold representation and supports Riemannian optimization. Following [24], [25], we summarize the key definitions used in this work.

A. Poincaré Ball Model

The d -dimensional Poincaré ball with curvature $c > 0$ is $\mathbb{B}^{d,c} = \{\mathbf{x} \in \mathbb{R}^d \mid c\|\mathbf{x}\|^2 < 1\}$, equipped with the conformal metric $g_{\mathbf{x}} = \lambda_{\mathbf{x}}^2 g_E$, $\lambda_{\mathbf{x}} = 2/(1 - c\|\mathbf{x}\|^2)$, and g_E denotes the standard Euclidean inner product. The conformal factor $\lambda_{\mathbf{x}}$ controls geometric distortion and is central to defining exponential and logarithmic maps. We use a learnable curvature, parameterized as $c = \text{softplus}(r_c) + \epsilon$, with trainable r_c and a small $\epsilon > 0$, ensuring that the curvature remains strictly positive during training.

B. Hyperbolic Operations at the Origin

All computations are performed in the tangent space at the origin $\langle \mathbf{0} \rangle$ for numerical stability [24].

- **Exponential and logarithmic map:** The exponential map projects the tangent vector v onto the hyperbolic manifold, while the logarithmic map performs the inverse operation by lifting hyperbolic points to the Euclidean space.

$$\begin{aligned} \exp_{\langle \mathbf{0} \rangle}^c(v) &= \tanh(\sqrt{c}\|v\|) \frac{v}{\sqrt{c}\|v\|}, \\ \log_{\langle \mathbf{0} \rangle}^c(x) &= \frac{1}{\sqrt{c}} \operatorname{artanh}(\sqrt{c}\|x\|) \frac{x}{\|x\|} \end{aligned} \quad (1)$$

- **Möbius addition** (\oplus_c): This defines the gyrovector structure supporting hyperbolic vector operations.

$$x \oplus_c y = \frac{(1 + 2c\langle x, y \rangle + c\|y\|^2)x + (1 - c\|x\|^2)y}{1 + 2c\langle x, y \rangle + c^2\|x\|^2\|y\|^2}. \quad (2)$$

- **Möbius matrix–vector multiplication** (\otimes_c): This enables linear transformations in hyperbolic space.

$$W \otimes_c x = \exp_{\langle \mathbf{0} \rangle}^c(W \log_{\langle \mathbf{0} \rangle}^c(x)). \quad (3)$$

- **Wrapped activation** (σ^{\otimes_c}): This applies nonlinear function (σ) while keeping outputs on the manifold.

$$\sigma^{\otimes_c}(x) = \exp_{\langle \mathbf{0} \rangle}^c(\sigma(\log_{\langle \mathbf{0} \rangle}^c(x))). \quad (4)$$

III. PROBLEM FORMULATION

Let $\mathcal{U} = \{u_1, \dots, u_n\}$ denote the set of n users, and $\mathcal{S} = \{s_1, \dots, s_m\}$ the set of m services, with each associated with their context information, including the geographical region (RG) and autonomous system (AS).

Assume $\mathcal{Q} = \{\mathcal{Q}^1, \mathcal{Q}^2, \dots, \mathcal{Q}^P\}$ is the set of P QoS parameters, where each $\mathcal{Q}^p \in \mathbb{R}^{n \times m}$ denotes partially observed user-service interactions matrix with entries

$$Q_{ij}^p = \begin{cases} q_{ij}^p > 0, & \text{if user } u_i \text{ invokes service } s_j, \\ 0, & \text{otherwise.} \end{cases} \quad (5)$$

TABLE I: Key notations.

Symbol	Description
n, m, P	Number of user, service, and QoS parameter
\mathcal{U}, \mathcal{S}	Set of user, and service
$\mathbb{B}^{d,c}$	d -dimensional Poincaré ball with curvature c
$\exp^c_{\langle 0 \rangle}, \log^c_{\langle 0 \rangle}$	Exponential, and logarithmic maps at origin
\mathcal{G}^p	QoS invocation graph for \mathcal{Q}^p
$\mathcal{G}^r, \mathcal{G}^a$	Region and AS context graphs
$\mathbb{G}_u^p, \mathbb{G}_s^p$	User and service hypergraphs
$\hat{\mathcal{A}}^i$	Normalized adjacency ($i \in \{r, a, \{1, \dots, P\}\}$)
$\hat{\mathbb{A}}_u^p, \hat{\mathbb{A}}_s^p$	Normalized hypergraph adjacencies
\mathcal{F}^i	Initial feature matrix ($i \in \{r, a, \{1, \dots, P\}\}$)
$\{\mathcal{V}^p\}_{p=1}^P, \mathcal{V}^r, \mathcal{V}^a$	QoS and context specific features
\mathcal{Z}^p	Gated-fusion output
$\hat{\mathcal{Q}}^p$	Predicted QoS matrix for p -th QoS parameter

The objective of this paper is to design a joint QoS prediction framework that learns a single model to predict all P QoS parameters simultaneously.

Table I provides a summary of the key notation used throughout the paper.

IV. METHODOLOGY

Fig. 1 illustrates the SHARP-QoS framework, comprising four key stages: (i) *Preprocessing*, which constructs the QoS and context graphs and generates initial node features via matrix factorization and one-hot encoding; (ii) *Hierarchical Feature Extraction Block (HFEB)*, learning QoS and context specific representations using hyperbolic graph convolution; (iii) *Feature Sharing and Fusion Block (FSFB)*, which adaptively fuses QoS-based and contextual features across QoS parameters using a subnetwork-routing strategy and gated fusion; (iv) *Joint QoS Prediction Module (JQPM)*, to achieve joint QoS prediction via a feed-forward network (FFN), and matrix product, while training under EMA-based loss balancing to mitigate negative transfer.

Note that all hyperbolic computations follow the Poincaré ball formulation in Sec. II, whereas feature sharing, fusion, and QoS prediction operate in Euclidean space.

A. Preprocessing

We first build the propagation graphs and initialize node features from the QoS matrices and context attributes.

1) *QoS- and Context-Graph Construction*: Learning on graphs can substantially improve QoS prediction; however, prior methods either relied on fully connected structures or used QoS/context graphs [11] with noisy or uninformative connections, limiting representation learning. To address this, our framework employs both QoS-invocation graphs and context graphs, defined as follows.

Definition IV.1 (QoS Invocation Graph (\mathcal{G}^p)). *Given a QoS matrix \mathcal{Q}^p , $p \in \{1, \dots, P\}$, the invocation graph $\mathcal{G}^p = \{\mathcal{V}, \mathcal{E}^p\}$ is a bipartite graph, where an edge $(u_i, s_j) \in \mathcal{E}^p$ exists iff $\mathcal{Q}_{ij}^p > 0$, indicating that user u_i invoked service s_j .*

Definition IV.2 (Context Graphs ($\mathcal{G}^r, \mathcal{G}^a$)). *For each context attribute $i \in \{r, a\}$, we define $\mathcal{G}^i = (\mathcal{V}, \mathcal{E}^i)$, where edges connect entities sharing the same region (r) or AS (a) attribute.*

The graph \mathcal{G}^p captures collaborative QoS usage patterns, while \mathcal{G}^r encodes coarse geographical proximity, and \mathcal{G}^a

captures fine-grained infrastructural priors (e.g., routing and peering). Although \mathcal{G}^r may subsume many connections in \mathcal{G}^a , the two provide complementary geographic and network-structural perspectives. Empirically, combining $\{\mathcal{G}^p, \mathcal{G}^r, \mathcal{G}^a\}$ enhances representation learning while preserving user-service privacy, as only global contextual attributes are used (excluding sensitive information such as IP, GPS coordinates, or provider identity).

We represent each graph using its adjacency matrix \mathcal{A}^i , $i \in \{r, a, \{1, \dots, P\}\}$, producing $P+2$ matrices of size $N \times N$, where $N = n+m$. Directly using these matrices in GCNs [26] may cause numerical instability due to high-degree nodes and missing self-information. Thus, we adopt symmetrically normalized adjacency matrices:

$$\hat{\mathcal{A}}^i = (\mathcal{D}^i)^{-1/2} \cdot (\mathcal{A}^i + \mathcal{I}) \cdot (\mathcal{D}^i)^{-1/2}, \quad \mathcal{D}_{jj}^i = \sum_k \mathcal{A}_{jk}^i, \quad (6)$$

where \mathcal{D}^i is the degree matrix and \mathcal{I} adds self-loops to preserve node self-features.

2) *Initial Features Extraction*: We derive initial node features using the sparse QoS matrices and the contextual attributes (RG, AS).

(i) **QoS-based features**: To obtain QoS features for each user and service node, we apply nonnegative matrix factorization [27] to each QoS parameter p , as shown in Eq. 7, yielding two low-rank matrices: the user feature matrix $\mathcal{F}_u^p \in \mathbb{R}^{n \times d_1}$ and the service feature matrix $\mathcal{F}_s^p \in \mathbb{R}^{m \times d_1}$.

$$\mathcal{F}_u^p, \mathcal{F}_s^p \leftarrow \mathcal{Q}^p \quad \text{such that} \quad \mathcal{F}_u^p \cdot (\mathcal{F}_s^p)^\top \approx \mathcal{Q}^p \quad (7)$$

(ii) **Context-based features**: To generate contextual embeddings for each user and service node, we employ one-hot encoding on RG and AS categories. Since one-hot vectors scale linearly with the number of categories and thus become high-dimensional, we use four autoencoders (AE) [28] with an identical feature dimension d_2 to obtain compact representations. This produces four contextual feature matrices: user features $\mathcal{F}_u^r, \mathcal{F}_u^a \in \mathbb{R}^{n \times d_2}$ and service features $\mathcal{F}_s^r, \mathcal{F}_s^a \in \mathbb{R}^{m \times d_2}$ corresponding to RG and AS contexts.

We then form the combined node feature matrix for each source $i \in \{r, a, \{1, \dots, P\}\}$ by concatenating the user and service features row-wise, yielding $\mathcal{F}^i \in \mathbb{R}^{N \times d}$.

B. Hierarchical Feature Extraction Block (HFEB)

Previous approaches [11], [18], [20] employing graph convolution or attention networks (GCN/GAT) aggregate information from neighboring nodes in Euclidean space to extract higher-order features for QoS prediction. However, Euclidean aggregation fails to capture the inherent hierarchical structure present in QoS and contextual data, leading to high distortion and suboptimal representations. To address this limitation, we adopt the hyperbolic formulations described in Sec. II, enabling graph representation learning in the Poincaré ball $\mathbb{B}^{d,c}$, where feature transformations and nonlinearities are realized via Möbius operations. Empirically, this yields more expressive representations by exploiting the underlying hierarchical structure, outperforming prior Euclidean approaches.

Specifically, we propose a dual hierarchical feature extraction mechanism, which is separately employed on the QoS and context graphs, as detailed subsequently.

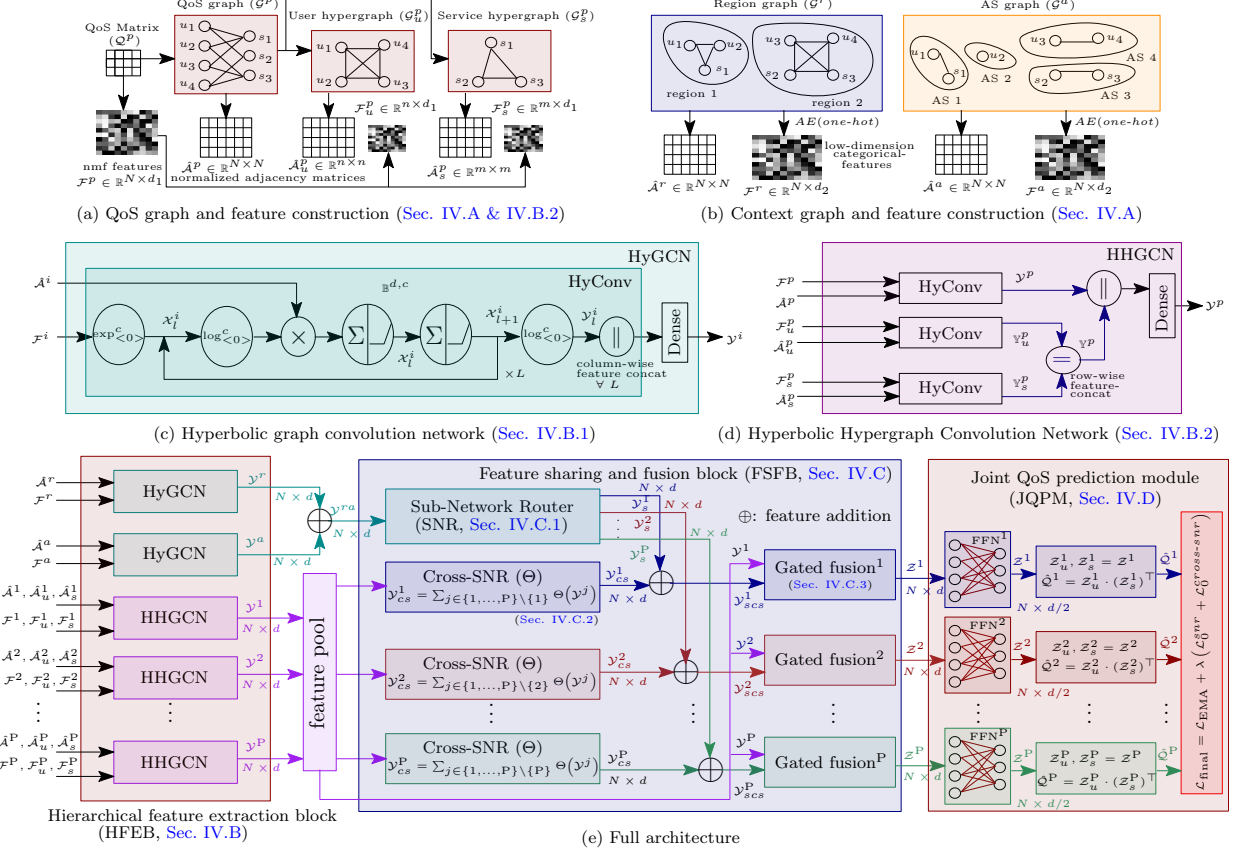


Fig. 1: SHARP-QoS: Overall framework.

1) Hyperbolic Graph Convolution Network (HyGCN):

Following [24], [25] (summarized in Sec. II), we adopt a Hyperbolic Graph Convolution Network (HyGCN) to extract hierarchical features from the context graphs \mathcal{G}^r and \mathcal{G}^a .

Given an initial feature matrix \mathcal{F}^i and normalized adjacency \hat{A}^i , where $i \in \{r, a\}$, HyGCN employs hyperbolic convolution (HyConv) unit that comprises two core operations, as depicted in Fig. 1 (c). Before using HyConv operations, we project the initial features to the hyperbolic manifold, $\mathcal{X}_0^i = \exp_{<0>}^c(\mathcal{F}^i)$. Following this, it first applies hyperbolic graph convolution, executing Euclidean message passing [26] in the tangent space. Secondly, a hyperbolic nonlinear transformation is performed through Möbius linear mapping and wrapped activation with ReLU. The process is defined in Eq. 8:

$$\begin{aligned} \mathcal{X}_l^i &= \sigma^{\otimes c} \left(\exp_{<0>}^c \left(\hat{A}^i \log_{<0>}^c (\mathcal{X}_l^i) \mathcal{W}_{l1}^i \right) \oplus_c \exp_{<0>}^c (b_{l1}) \right), \\ \mathcal{X}_{l+1}^i &= \sigma^{\otimes c} \left(\exp_{<0>}^c \left(\log_{<0>}^c (\mathcal{X}_l^i) \mathcal{W}_{l2}^i \right) \oplus_c \exp_{<0>}^c (b_{l2}) \right). \end{aligned} \quad (8)$$

Here, $\mathcal{W}_{l1}^i \in \mathbb{R}^{d \times 2d}$ and $\mathcal{W}_{l2}^i \in \mathbb{R}^{d \times d}$ are learnable weights, with corresponding biases $b_{l1} \in \mathbb{R}^{2d}$ and $b_{l2} \in \mathbb{R}^d$. We then return to Euclidean space via $\mathcal{Y}_l^i = \log_{<0>}^c (\mathcal{X}_l^i) \in \mathbb{R}^{N \times d}$.

HyGCN stack L HyConv layers whose outputs are concatenated column-wise, and then a nonlinear transformation layer is applied with learnable weight matrix $\mathcal{W}_1^i \in \mathbb{R}^{d(L+1) \times d}$ with an activation function σ_1 , as shown in Eq. 9, to obtain the higher-order hierarchical features. Note that this operation is performed entirely in Euclidean space.

$$\mathcal{Y}^i = \sigma_1 \left(\left| \begin{array}{l} \vdots \\ \mathcal{Y}_l^i \\ \vdots \end{array} \right| \right) \cdot \mathcal{W}_1^i \quad (9)$$

We independently employ HyGCN over \mathcal{G}^r and \mathcal{G}^a , yielding hierarchical contextual features $\mathcal{Y}^r \in \mathbb{R}^{N \times d}$ and $\mathcal{Y}^a \in \mathbb{R}^{N \times d}$. Adding $\mathcal{Y}^{ra} = \mathcal{Y}^r + \mathcal{Y}^a$ provides the aggregated region and network-aware, structural contextual features, which we used in Sec. IV-C.

2) Hyperbolic Hypergraph Convolution Network (HHGCN): Adopting HyGCN directly for QoS-based graphs \mathcal{G}^p for each QoS parameter p , may result in suboptimal QoS-based hierarchical features due to weak structural information owing to its sparse or noisy QoS interactions. We therefore augment the bi-partite structural signals using user- and service-based hypergraphs. The user-based hypergraph \mathcal{G}_u^p is defined as follows:

Definition IV.3 (User Hypergraph (\mathcal{G}_u^p)). *Given a QoS invocation graph \mathcal{G}^p , we derive user (service) hypergraph defined as $\mathcal{G}_u^p = \{\mathbb{V}_u^k, \mathbb{E}_u^k\}$ where $\mathbb{V}_u^k \in \mathcal{U}$ and $\mathbb{E}_u^k = \{e_1, e_2, \dots, e_m\}$ are user set and hyperedge set, respectively.*

The service-based hypergraph \mathcal{G}_s^p is obtained in a similar manner. Notably, \mathcal{G}_u^p and \mathcal{G}_s^p are constructed via a second-hop traversal on \mathcal{G}^p with incidence matrix \mathcal{H}^p . Consequently, we obtain the normalized adjacency matrices $\hat{\mathcal{A}}_u^p \in \mathbb{R}^{n \times n}$ and $\hat{\mathcal{A}}_s^p \in \mathbb{R}^{m \times m}$ for each graphs \mathcal{G}_u^p and \mathcal{G}_s^p , respectively, as shown in Eq. 10.

$$\begin{aligned} \hat{\mathcal{A}}_u^p &= (\mathbb{D}_u^p)^{-1/2} \cdot \mathcal{H}^p \cdot (\mathbb{D}_s^p)^{-1} \cdot (\mathcal{H}^p)^\top \cdot (\mathbb{D}_u^p)^{-1/2}, \\ \hat{\mathcal{A}}_s^p &= (\mathbb{D}_s^p)^{-1/2} \cdot (\mathcal{H}^p)^\top \cdot (\mathbb{D}_u^p)^{-1} \cdot \mathcal{H}^p \cdot (\mathbb{D}_s^p)^{-1/2} \end{aligned} \quad (10)$$

Here, \mathbb{D}_u^p and \mathbb{D}_s^p are degree matrices obtained using the \mathbb{A}_u^p and \mathbb{A}_s^p via hypergraphs \mathbb{G}_u^p and \mathbb{G}_s^p , respectively.

We employ Hyperbolic Hypergraph Convolution Network (HHGCN), shown in Fig. 1 (d), leveraging the HyConv formulations (see Eq. 8–9) to each QoS graphs/hypergraphs \mathcal{G}^p , \mathbb{G}_u^p and \mathbb{G}_s^p independently, and resulting outputs are then bring to Euclidean space producing \mathcal{Y}_l^p , \mathbb{Y}_{ul}^p and \mathbb{Y}_{sl}^p , respectively. \mathbb{Y}_{ul}^p and \mathbb{Y}_{sl}^p are first concatenated in a row-wise manner, whose output is then concatenated column-wise with \mathcal{Y}_l^p . The final consolidated features are obtained by employing a non-linear transformation with learnable weights $\mathcal{W}_2^p \in \mathbb{R}^{2d(l+1) \times d}$ and an activation function σ_1 , as shown in Eq. 11.

$$\mathcal{Y}^p = \sigma_1 \left(\parallel_{l=0}^L (\mathcal{Y}_l^p \parallel [\mathbb{Y}_{ul}^p; \mathbb{Y}_{sl}^p]) \cdot \mathcal{W}_2^p \right) \quad (11)$$

The resulting output $\mathcal{Y}^p \in \mathbb{R}^{N \times d}$ encodes QoS-based hierarchical features for p -th QoS parameter, which is utilized in the next section.

C. Feature Sharing and Fusion Block (FSFB)

This section presents our approach to controlled feature sharing based on representations learned via HyGCN and HHGCN for joint QoS prediction. Since feature sharing is an algorithmic design choice rather than geometric modeling, all operations in this stage are performed in Euclidean space.

Existing joint QoS prediction methods [20], [15], [19], [21], [16], [18] suffer from limited flexibility in parameter sharing or computational overhead. Hard parameter sharing forces all tasks to share early layers, often causing negative transfer, while soft parameter sharing relies on task-specific parameters with similarity regularization, increasing model complexity and limiting scalability. To address these issues, inspired by [22], we introduce a subnetwork routing strategy that enables adaptive, task-specific feature sharing through selective routing over shared subnetworks.

1) *Subnetwork Routing (SNR) Mechanism*: In our proposed SHARP-QoS framework, QoS and context features are shared in distinct ways. We first explain the Sub-Network Routing Mechanism (SNR) [22] for contextual features $\mathcal{Y}^{ra} \in \mathbb{R}^{N \times d}$ obtained via HyGCNs (Sec. IV-B1). We dynamically select and aggregate a sparse subset of transformed features conditioned on the target task. To achieve this, SNR router first process \mathcal{Y}^{ra} through K_1 parallel blocks $\{\phi_k(\cdot)\}_{k=1}^{K_1}$, each comprise layer normalization (LN), non-linear transformation with ReLU activation (Dense), as shown in Eq. 12.

$$\phi_k(\mathcal{Y}^{ra}) = \text{Dense}_k(\text{LN}(\mathcal{Y}^{ra})), \quad \phi_k(\mathcal{Y}^{ra}) \in \mathbb{R}^{N \times d_o} \quad (12)$$

where d_o is the output dimension. We further employ a QoS parameter specific linear transformation with \mathcal{W}_k^p , helping to enhance the task specificity, as shown in Eq. 13.

$$\tilde{\phi}_k^p(\mathcal{Y}^{ra}) = \phi_k(\mathcal{Y}^{ra}) \cdot \mathcal{W}_k^p, \quad (13)$$

where $\mathcal{W}_k^p \in \mathbb{R}^{d_o \times d_o}$ is learned independently. To enable adaptive feature sharing for each QoS parameter, we maintain learnable coding variables $\{c_k^p\}_{p=1}^P$ per block, controlling the connection. Specifically, we draw each c_k^p from a Bernoulli distribution π_k^p , owing to its discrete nature, it does not allow efficient gradient-based learning. To address this issue, we leverage hard concrete distribution [29], where each coding

variable c_k^p parameterized by a learnable logit $\log \alpha_k^p$, sampled using a uniform distribution $u \sim \mathcal{U}(0, 1)$.

$$\begin{aligned} s &= \sigma_2 \left((\log u - \log(1-u) + \log \alpha_k^p) / \tau \right) \\ c_k^p &= \text{clip}(\bar{s}, 0, 1), \quad \bar{s} = s(\gamma - \beta) + \beta \end{aligned} \quad (14)$$

Here, σ_2 is an activation function, $\beta < 0, \gamma > 1$ define the stretching interval, and τ controls the smoothness. Subsequently, we obtain the QoS parameter-specific features by using a sparsely weighted aggregation using the coding variable c_k^p , as illustrates in Eq. 15.

$$\mathcal{Y}_s^p = \frac{1}{\sum_{k=1}^K g_k^p} \sum_{k=1}^{K_1} c_k^p \tilde{\phi}_k^p(\mathcal{Y}^{ra}), \quad (15)$$

Here, normalization term helps prevent scale collapse when only a small number of blocks are activated, allowing fractional routing in training. During inference, we follow the hard selection where stochastic coding variables are replaced by deterministic binary activations by thresholding (δ), $c_k^p = \mathbb{I}[\sigma_2(\log \alpha_k^p) > \delta]$, yielding interpretable and task-specialized contextual features.

2) *Cross-SNR Routing Mechanism*: Since QoS parameters stem from common underlying network conditions, we argue that they either depend on or influence each other. However, at the same time, they may not have trended all the time. Previous studies have undermined these challenges and avoided sharing QoS-based features. Addressing this issue, we introduced cross-subnetwork routing (Cross-SNR) strategy to obtain the task-specialized QoS features, exploiting the shareable component within the QoS-based features for other QoS parameters. Cross-SNR $\Theta(\cdot)$ employs the same formulations, as in Eqs. 12–15 with K_2 number of blocks, on QoS features pool $\{\mathcal{Y}^p\}_{p=1}^P$ derived using HHGCNs (Eq. 11). For each target QoS parameter p , we construct a shared representation by excluding its own feature and summing the remaining $P-1$ task-specialized QoS features outputs, as shown in Eq. 16.

$$\mathcal{Y}_{cs}^p = \sum_{j \in \{1, \dots, P\} \setminus \{p\}} \Theta(\mathcal{Y}^j) \quad (16)$$

We further obtain the combined shared features $\mathcal{Y}_{scs}^p = \mathcal{Y}_s^p + \mathcal{Y}_{cs}^p$ by summing task-specialized contextual and QoS features, yielding multi-context shared features, enriched in the network, geographical, and QoS dynamics.

3) *Gated-feature Fusion Module*: This module introduces the adaptive strategy to combine the shared task-specific representations $\mathcal{Y}_{scs}^p \in \mathbb{R}^{N \times d}$ with the structure-aware QoS features $\mathcal{Y}^p \in \mathbb{R}^{N \times d}$ (computed in Eq. 11, Fig. 1 (e)). Specifically, we introduce a gated feature fusion mechanism, which learn a gating weight \mathcal{W}_g^p with an activation function σ_2 producing the resulting gates g^p for each QoS parameter p , as shown in Eq. 17. The gates g^p enable the model to adaptively balance structural and multi-context shared information, illustrated in Eq. 18, where \odot represents the element-wise multiplication. The resulting feature \mathcal{Z}^p is then forwarded for the downstream QoS prediction task.

$$g^p = \sigma_2 ([\mathcal{Y}^p \parallel \mathcal{Y}_{scs}^p] \cdot \mathcal{W}_g^p) \quad (17)$$

$$\mathcal{Z}^p = g^p \odot \mathcal{Y}^p + (1 - g^p) \odot \mathcal{Y}_{scs}^p \quad (18)$$

D. Joint QoS Prediction Module (JQPM)

To enable the joint learning, we obtain task-specific feed-forward networks $\text{FFN}^p(\cdot)$ for each QoS parameter p , which comprises two dense layers with ReLU and Linear activation, respectively. Subsequently, the resulting features \mathcal{Z}^p is split into QoS parameter specific user feature matrix \mathcal{Z}_u^p and service feature matrix \mathcal{Z}_s^p . We employ the matrix multiplication on \mathcal{Z}_u^p and \mathcal{Z}_s^p , providing the predicted QoS matrix $\hat{\mathcal{Q}}^p$. This formulation is illustrated in Eqs. 19-20.

$$\mathcal{Z}^p = \text{FFN}^p(\mathcal{Z}^p), \quad \mathcal{Z}_u^p, \mathcal{Z}_s^p = \mathcal{Z}^p \quad (19)$$

$$\hat{\mathcal{Q}}^p = \mathcal{Z}_u^p \cdot (\mathcal{Z}_s^p)^\top \quad (20)$$

1) *Objective Function and Loss Scale Balancing*: Owing to network instability, QoS data may contain outliers; therefore, we train our model using a robust loss function, Mean Absolute Error (MAE), illustrated in Eq. 21.

$$\mathcal{L}^p = \frac{1}{|\text{TD}|} \sum_{(i,j) \in \text{TD}} |\mathcal{Q}_{ij}^p - \hat{\mathcal{Q}}_{ij}^p| \quad (21)$$

Here, TD denotes the training density, ensuring only observed QoS values contribute to the loss calculation.

We argue that the combined loss $\sum_{p=1}^P \mathcal{L}^p$ is prone to be dominated by a few QoS parameters that yield larger error magnitudes, which might lead to negative transfer across tasks. This problem can be attributed to the numerical ranges of QoS parameters (see Table II). Recent studies PMT [16] and WAMTL [21] employed heteroscedastic uncertainty weighting (HUW) and Dynamic Weight Averaging (DWA), respectively, to rescale task losses. However, they tend to suffer from instability during the early training stages and exhibit slow adaptation to QoS dynamics. To address this issue, we introduce an EMA-based loss scaling strategy that moderates task contributions while suppressing short-term fluctuations.

Specifically, at i -th training iteration, we estimate the smoothed loss $\tilde{\mathcal{L}}_i^p$ using a smoothing coefficient $\beta \in [0, 1]$, controlling the moving average momentum. The normalized QoS parameter specific weights w^p are then computed by inverting the smoothed losses, as shown in Eq. 22. Here, $\tilde{\mathcal{L}}_0^p = 1$ and ϵ is a small constant for numerical stability.

$$\tilde{\mathcal{L}}_i^p = \beta \tilde{\mathcal{L}}_{(i-1)}^p + (1 - \beta) \mathcal{L}_i^p, \quad w^p = \frac{(\tilde{\mathcal{L}}^p + \epsilon)^{-1}}{\sum_{p=1}^P (\tilde{\mathcal{L}}^p + \epsilon)^{-1}}. \quad (22)$$

The resulting joint loss is expressed as $\mathcal{L}_{\text{EMA}} = \sum_{p=1}^P w^p \mathcal{L}^p$. We further introduce a \mathcal{L}_0 -based regularization term, encouraging the sparsity in the routing block selection. The final joint objective function is illustrated in Eq. 23, utilizes to train our model. Note that the regularization coefficient λ controls the trade-off between QoS-specific prediction accuracy and the sparsity across feature routing networks.

$$\mathcal{L}_{\text{final}} = \mathcal{L}_{\text{EMA}} + \lambda (\mathcal{L}_0^{\text{snr}} + \mathcal{L}_0^{\text{cross-sn}}) \quad (23)$$

Overall, our framework ensures that EMA-based balancing demonstrates smooth QoS dynamics, stable, and adaptive weighting. Further, combining with the sparse routing regularizer achieves effective feature sharing across QoS parameters, leading to balanced multi-task optimization, with improved QoS prediction performance. The complexity analysis of SHARP-QoS is illustrated in Appendix A of supp. file.

TABLE II: Datasets statistics.

Attributes		WSDREAM-2T [23]	Small-3T [16]	gRPC-4T [14]
No. of User and Service		339, 5825	112, 36	57, 150
No. of User's Region and AS		31, 137	24, 80	13, 16
No. of Service's Region and AS		74, 2699	16, 28	1, 1
No. of QoS Invocation		1831253	2870	8550
Response Time (RT)	Range (min, max) mean \pm std	(0.0010, 19.9900) 0.9086 \pm 1.9727	(0.0011, 25.806) 1.2667 \pm 2.5234	-
Throughput (TP)	Range (min, max) mean \pm std	(0.0040, 1000.0000) 47.5617 \pm 110.970	(0.648, 3454.468) 35.0903 \pm 132.533	-
Reliability (RE)	Range (min, max) mean \pm std	- -	(0.001, 1.0) 0.9897 \pm 0.0592	(44.61%, 99.99%) 68.38% \pm 11.26
Cost (CT)	Range (min, max) mean \pm std	- -	- -	(4.6000, 17.6000) 11.2214 \pm 1.9538
Latency (LT)	Range (min, max) mean \pm std	- -	- -	(0.0484, 151.8636) 3.7787 \pm 9.5216
Power (PW)	Range (min, max) mean \pm std	- -	- -	(17.2100, 92.7500) 56.5041 \pm 20.0000

V. EXPERIMENTAL RESULTS

We implement our framework using TensorFlow 2.19.0 with Python 3.12.7. All experiments were conducted on an Ubuntu 24.04.2 LTS (Linux kernel 5.15.0-139-generic, x86_64) equipped with a 12th Gen Intel(R) Core(TM) i7-12700 CPU @ 1.42 GHz and 130 GiB RAM.

A. Experimental Setup

Datasets: To evaluate SHARP-QoS, we employ three real-world web services datasets: (i) WSDREAM-2T: A public benchmark comprises two QoS parameters, response time (RT) and throughput (TP), for 339 users and 5825 services with geographical and network information [23]. (ii) Small-3T: This dataset includes three QoS parameters, RT, TP, and reliability (RE), for 112 users and 36 services, with details on the network and geographical attributes [16]. (iii) gRPC-4T: Collected for Autonomous Vehicle (AV)-related services, this dataset comprises four QoS parameters, RE, cost (CT), latency (LT), and power (PW), for 57 users across 27 cities and 150 gRPC-based services deployed on five academic servers [14]. Table II provides statistical characteristics of these datasets.

Train-test splits: To simulate realistic sparse dataset scenarios, we randomly sample and remove a fixed percentage $\text{TD} \in \{5, 10, 15, 20\}\%$ of the QoS records from each dataset, where TD represents training density. The remaining $y_{\text{test}} = (100 - \text{TD})\%$ is used for performance evaluation. To ensure statistical reliability, we conducted multiple runs of model training and reported the average results.

TABLE III: Parameters configuration.

Attributes		Value
NMF/Autoencoder	d_1/d_2 dimension	128
	No. of layers (L)	2
HyGCN/HHGCN	W_{i1}^t/W_{i2}^t dimension	128 \times 128
	W_1^t dimension	256 \times 128
	Activation function σ_1	ReLU
	No. of Blocks (K_1/K_2)	4
SNR/ Cross-SNR	W_k^p dimension	64 \times 128
	Activation function (σ_2)	sigmoid
	Activation threshold (δ)	0.5
Gated Fusion	W_g^p dimension	32 \times 256
	Activation function (σ_2)	sigmoid
FFN	W_1 dimension	128 \times 128
	W_2 dimension	128 \times 64
	Activation function	ReLU, Linear
Objective Function	EMA coefficient (β)	0.99
	Regularization coefficient (λ)	1×10^{-5}
Training Parameters	No. of Epoch	10000
	Optimizer	AdamW
	Learning rate	1×10^{-3}
	Decay rate	1×10^{-4}
	Patience	400

TABLE IV: Performance comparison with joint QoS prediction methods.

		WSDREAM-2T Dataset							
QoS Para.	Method	MAE				RMSE			
		5	10	15	20	5	10	15	20
RT	JQSP [18]	0.5079	0.4406	0.4154	0.4072	1.9491	1.4445	1.3496	1.3181
	WAMTL [21]	0.4652	0.4097	0.3844	0.3663	1.3607	1.2800	1.2345	1.2017
	DNM [15]	0.4121	0.3621	0.3471	0.3214	1.3866	1.2670	1.2216	1.2070
	MGEN [19]	0.4115	0.3423	0.3289	0.3181	1.3579	1.2602	1.2189	1.1950
	SHARP-QoS	0.3668	0.3243	0.3099	0.2930	1.3116	1.2450	1.1979	1.1516
	$I(\%)$	10.86	5.25	5.78	7.89	3.41	1.21	1.72	3.63
TP	JQSP [18]	21.9919	17.9796	16.8000	14.3989	79.5323	54.0659	49.8281	49.0998
	WAMTL [21]	18.8521	15.3414	14.5306	13.7570	54.5032	46.7399	43.5842	41.5083
	DNM [15]	17.2980	14.0650	14.5436	14.1170	58.1629	50.3930	49.8868	46.9100
	MGEN [19]	15.4529	13.0833	12.6516	12.3941	50.7213	43.3581	43.2147	42.1618
	SHARP-QoS	13.2402	11.4814	10.8035	10.4069	47.0426	41.7156	39.7392	38.7746
	$I(\%)$	14.32	12.24	14.61	16.03	7.25	3.79	8.04	6.59
Small-3T Dataset									
RT	DNM [15]	1.1098	1.0413	1.0332	1.0016	2.4307	2.1130	2.0288	2.0040
	JQSP [18]	0.7688	0.5053	0.4495	0.4650	1.6266	1.3327	1.0606	1.1111
	MGEN [19]	0.6627	0.4216	0.3794	0.3639	1.4639	1.1895	1.0862	1.0790
	WAMTL [21]	0.6562	0.4771	0.4423	0.4093	1.2595	1.2268	1.1525	1.1269
	SHARP-QoS	0.4496	0.3945	0.3099	0.2871	1.1652	1.1015	1.0263	1.0029
	$I(\%)$	31.48	6.43	18.32	21.10	7.49	7.40	3.23	7.05
TP	JQSP [18]	54.2766	46.9502	50.9577	27.0942	253.2556	218.3714	112.5865	92.1144
	DNM [15]	43.2913	33.4560	35.6610	34.6610	116.1662	109.6389	106.0478	102.7562
	WAMTL [21]	33.6497	27.6057	23.2590	18.9285	132.5707	129.2284	126.6743	111.6510
	MGEN [19]	24.5219	18.1270	15.0493	14.9293	137.2764	107.0232	99.8948	78.2624
	SHARP-QoS	24.4732	17.7958	14.4464	11.4730	88.3392	71.9799	72.4821	43.4623
	$I(\%)$	0.20	1.83	4.01	23.15	23.95	32.74	27.44	44.47
RE	WAMTL [21]	0.2805	0.0941	0.0907	0.0699	0.3528	0.1383	0.1148	0.1094
	MGEN [19]	0.0484	0.0395	0.0164	0.0158	0.1926	0.1830	0.0972	0.0964
	JQSP [18]	0.0429	0.0348	0.0181	0.0116	0.0776	0.0662	0.0455	0.0426
	DNM [15]	0.0112	0.0109	0.0101	0.0091	0.0572	0.0547	0.0484	0.0459
	SHARP-QoS	0.0100	0.0072	0.0062	0.0060	0.0344	0.0339	0.0326	0.0299
	$I(\%)$	10.71	33.94	38.61	34.07	39.86	38.03	28.35	29.81
gRPC-4T Dataset									
RE	WAMTL [21]	0.0475	0.0360	0.0290	0.0240	0.0688	0.0498	0.0423	0.0325
	JQSP [18]	0.0879	0.0753	0.0654	0.0626	0.1545	0.1329	0.1226	0.1139
	DNM [15]	0.0505	0.0345	0.0328	0.0310	0.0663	0.0495	0.0476	0.0449
	MGEN [19]	0.0422	0.0287	0.0253	0.0233	0.0706	0.0564	0.0440	0.0413
	SHARP-QoS	0.0295	0.0200	0.0160	0.0123	0.0443	0.0475	0.0416	0.0286
	$I(\%)$	30.09	30.31	36.76	47.21	33.18	4.04	5.45	30.75
CT	WAMTL [21]	1.1504	0.9515	0.7851	0.6334	1.4946	1.2406	1.0152	1.0023
	MGEN [19]	1.5543	1.1733	0.8303	0.7219	2.2099	1.5409	1.1259	0.9951
	DNM [15]	1.1464	0.8296	0.6902	0.6659	1.5566	1.1257	0.9239	0.8922
	JQSP [18]	1.0381	0.8232	0.7807	0.7852	1.3539	1.0784	1.0124	0.9981
	SHARP-QoS	0.8836	0.7060	0.6008	0.5618	1.2044	0.9976	0.8452	0.8020
	$I(\%)$	14.88	14.24	12.95	15.63	11.04	7.49	8.52	10.11
LT	JQSP [18]	4.8826	3.9492	3.6310	3.3331	9.4759	7.7057	7.5593	7.4431
	DNM [15]	4.3804	4.2163	3.4580	3.4164	9.2961	8.3004	7.9792	7.9022
	MGEN [19]	2.6290	2.0706	2.0523	2.0584	9.0301	8.6840	8.4091	5.6198
	WAMTL [21]	2.5137	3.5620	3.4255	3.6652	7.7507	10.4098	10.418	10.7406
	SHARP-QoS	1.1910	0.8909	0.8241	0.7896	1.9780	1.7863	1.5810	1.5799
	$I(\%)$	52.62	56.97	59.85	61.64	74.48	76.82	79.09	71.89
PW	WAMTL [21]	12.8474	9.2137	8.4201	7.3705	17.8271	16.3605	14.3976	12.9835
	JQSP [18]	13.8065	10.5663	10.0520	9.7656	17.7371	13.9167	13.2140	12.6584
	MGEN [19]	12.4266	8.0331	6.2375	5.6198	19.7486	14.4056	12.0813	11.1539
	DNM [15]	12.2556	9.0397	8.5686	8.2758	17.3730	14.3611	12.5894	12.1153
	SHARP-QoS	11.3154	7.2178	6.2153	5.0122	16.8738	13.6852	12.0119	10.7687
	$I(\%)$	7.67	10.15	0.36	10.81	2.87	1.66	0.57	3.45

Para.:parameter

Evaluation Metrics: To evaluate the performance, we employ two widely used metrics: Mean Absolute Error (MAE), and Root Mean Square Error (RMSE), defined as follows:

$$\text{MAE} = \frac{1}{|y_{test}|} \sum_{q_{ij}^p \in y_{test}} |q_{ij}^p - \hat{q}_{ij}^p|,$$

$$\text{RMSE} = \sqrt{\frac{1}{|y_{test}|} \sum_{q_{ij}^p \in y_{test}} (q_{ij}^p - \hat{q}_{ij}^p)^2} \quad (24)$$

A lower error value indicates a higher prediction accuracy. In addition, we report the relative improvement metric I (in %) to compare the best-performing method M_1 with the second-best baseline M_2 , given by:

$$I(M_1, M_2) = ((P_2 - P_1) / P_2) \times 100\% \quad (25)$$

where P_1 and P_2 denote the performance scores (e.g., MAE, and RMSE) of M_1 and M_2 , respectively. A higher value of I indicates that M_1 outperforms M_2 .

Parameter Configurations: Unless specified otherwise, we use the hyperparameters listed in Table III.

B. Performance Comparison

Among all available joint QoS prediction baselines, we evaluated SHARP-QoS against [15], [18], [19], [21] via error metrics (MAE, RMSE) and computational efficiency. Comparison with PMT [16], and HTG [20] is discarded as they require topology-level AS-links data, which is publicly unavailable. To further strengthen our analysis, we compare with five single-parameter QoS prediction methods.

TABLE V: Computational Efficiency.

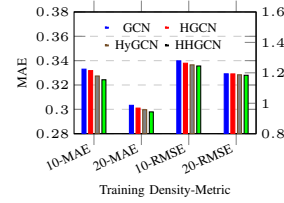
Method	Params (M)	FLOPs (G)	Train Time (sec.)	Inference Time (sec.)
MGEN [19]	1.79	4774.56	3847.25	8.10×10^{-5}
WAMTL [21]	0.91	777.61	3901.07	1.35×10^{-5}
DNM [15]	2.44	211.8	2851.27	2.16×10^{-6}
JQSP [18]	2.02	90.12	2532.52	6.14×10^{-8}
SHARP-QoS	1.62	133.4	5516.00	3.97×10^{-8}

(i) Comparison with multi-task methods on error metrics: Table IV reports a comprehensive comparison of SHARP-QoS against state-of-the-art (SOTA) joint QoS prediction baselines across three datasets and four training densities (5% – 20%, step size 5%). While prior methods demonstrate inconsistent behavior across settings, our approach delivers uniformly superior performance, achieving average improvements of 19.47% in MAE and 19.32% in RMSE over second-best models across all datasets. We observed that performance gains become even more pronounced as the number of tasks increases. Specifically, our method surpasses existing approaches on WSDREAM-2T by 10.87% (MAE) and 4.46% (RMSE), on Small-3T by 18.65% (MAE) and 24.15% (RMSE), and on gRPC-4T by 28.88% (MAE) and 26.34% (RMSE). These results strongly highlight the scalability and generalization strength of our framework under multi-task expansion. Against MoE-based architectures such as MGEN [19] and WAMTL [21], our method secures substantial gains of 40.77% (MAE) and 40.99% (RMSE). We attribute this advantage to the stability of our design, in contrast to the load imbalance and expert collapse commonly observed in MoE-based training. JQSP, despite its graph-attention foundation, suffers from severe performance degradation, 47.66% in MAE and 35.91% in RMSE, due to its sensitivity to outliers. Likewise, DNM [15], though architecturally intricate, falls behind our method by 38.69% (MAE) and 29.43% (RMSE), reflecting its inability to mitigate negative transfer effectively. Collectively, these results affirm the superiority of SHARP-QoS, demonstrating strong resilience to outliers, effective suppression of negative transfer, and consistent hierarchical feature extraction across all datasets.

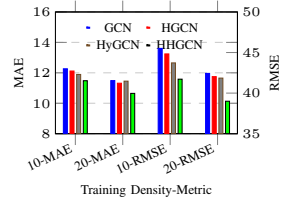
(ii) Comparison with multi-task methods on computational complexity: To evaluate computational efficiency, we compare our framework across four metrics: trainable parameters (Params), floating-point operations (FLOPs), training time, and inference time, as shown in Table V. While our model exhibits a slightly higher training time, it maintains moderate Params and FLOPs, and is the fastest among all baselines during inference. Importantly, training is performed offline; that is, the extended training time does not impact runtime service invocation or latency during deployment. Relative to WAMTL [21], which has the smallest parameter footprint ($1.78 \times$ fewer than ours), our method delivers substantial gains with $5.83 \times$ lower FLOPs and an outstanding $1000 \times$ speedup in inference. Likewise, compared to JQSP [18], which reports the lowest FLOPs (ours being only $1.48 \times$ higher), our framework achieves $1.55 \times$ faster inference while also requiring $1.25 \times$ fewer parameters. Notably, despite lower compute, our approach consistently achieves better predictive accuracy across all datasets. These results confirm that SHARP-QoS offers an advantageous trade-off between computational cost

TABLE VI: Performance comparison on single-task methods on WSDREAM-2T.

QoS Para.	Method	MAE		RMSE	
		10	20	10	20
RT	PMF [8]	0.4996	0.4492	1.2866	1.1828
	CMF [4]	0.4511	0.3767	1.5012	1.3633
	DCALF [30]	0.4544	0.4246	1.2450	1.1759
	IlmQoS [12]	0.3600	<u>0.3270</u>	<u>1.2240</u>	<u>1.1590</u>
	QoS GNN [11]	0.3450	-	1.2760	-
	SHARP-QoS	0.3243	0.2930	1.2450	1.1516
TP	$I(\%)$	5.22	9.65	-1.72	0.64
	CMF [4]	23.2347	18.8050	83.5279	76.5277
	PMF [8]	16.1755	14.6694	46.4439	42.4855
	DCALF [30]	15.3595	13.6697	45.9013	41.2194
	QoS GNN [11]	13.9460	-	47.9550	-
	IlmQoS [12]	12.0220	10.7600	42.9470	38.3650
	SHARP-QoS	11.4814	10.4069	41.7156	38.7746
	$I(\%)$	4.50	3.28	2.87	-1.07



(a) WSDREAM-2T (RT)



(b) WSDREAM-2T (TP)

Fig. 2: Impact of HHGCN module.

and performance, delivering high accuracy, reduced runtime overhead, and strong scalability, making it highly suitable for latency-critical and real-time QoS prediction systems.

(iii) Comparison with single-task methods: Table VI presents the comparison of SHARP-QoS with five recent single-task methods on the WSDREAM-2T. Our method consistently achieves the lowest MAE across all methods, demonstrating higher average prediction accuracy. However, in certain cases (RT-10, TP-20), our model achieves slightly higher RMSE, underperforms compared to underlined method. This may be attributed to their dedicated optimization for individual QoS parameters. Despite this, our approach provides a more nuanced solution by jointly optimizing multiple QoS parameters within a unified framework. This balance is highly relevant in real deployment scenarios, where service selection depends on multiple QoS properties rather than isolated metrics.

C. Model Ablation Study

This section analyzes the contribution of two key components of SHARP-QoS: (i) the hierarchical feature extraction via HHGCN, and (ii) the EMA-based loss scaling.

(i) Impact of Hierarchical Feature Extraction Block: Fig. 2 demonstrates that the proposed hyperbolic-hypergraph convolution (HHGCN) consistently outperforms the other three variants: standard Euclidean graph convolution (GCN), Euclidean hypergraph convolution (HGCN), and hyperbolic graph convolution (HyGCN). On the WSDREAM-2T (RT) dataset, HHGCN achieves improvements of 3.00% (MAE) and 3.07% (RMSE) over GCN, and 2.46% (MAE) and 2.44% (RMSE) over HGCN. Further, incorporating user/service hyper-edges yields additional gains over HyGCN (1.59% MAE and 1.79% RMSE). A more pronounced improvement is observed on the TP dataset: HHGCN surpasses GCN by 7.89% (MAE)

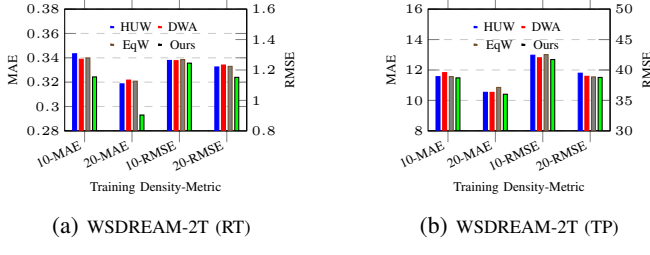


Fig. 3: Impact of EMA-based loss balancing.

TABLE VII: Module Ablation on WSDREAM-2T.

QoS Para.	Module	MAE		RMSE	
		10	20	10	20
RT	- HHGNNs - Cross-SNR	0.6229	0.6049	2.1301	1.9588
	- SNR - Cross-SNR	0.5275	0.5139	1.8966	1.8783
	- HHGNNs - SNR	0.3309	0.3258	1.2664	1.1987
	- SNR	0.3442	0.3154	1.2777	1.2237
	- HHGNNs	0.3395	0.3187	1.2728	1.2221
	- Cross-SNR	0.3345	0.3031	1.2638	1.1987
Ours		0.3243	0.2930	1.2450	1.1516
TP	- HHGNNs - Cross-SNR	31.5699	31.2864	96.6124	96.1364
	- SNR - Cross-SNR	28.8214	25.6720	83.9696	76.4003
	- HHGNNs - SNR	12.7072	18.8945	47.6640	62.3913
	- SNR	15.0648	14.0172	52.2302	48.9402
	- HHGNNs	17.5674	16.6736	58.8570	57.0896
	- Cross-SNR	13.1844	12.0310	48.9919	43.9704
Ours		11.4814	10.4069	41.7156	38.7746

and 8.47% (RMSE), HGCN by 6.64% (MAE) and 8.47% (RMSE), and HyGCN by 6.28% (MAE) and 5.96% (RMSE). These results demonstrate that HHGNN effectively captures hierarchical structure for QoS data and exploits hyper-edge relations to strengthen representation learning. Note that, HyGCN ablations for AS and RG graphs are omitted, as HyGCN was directly adopted based on empirical validation.

(ii) **Impact of EMA-Based Loss Scaling:** Fig. 3 compares different loss-balancing strategies, including homoscedastic uncertainty weighting (HUW) [16], dynamic weight averaging (DWA) [21], equal weighting (EqW), and our EMA-based approach. On WSDREAM-2T (RT, TP), our method outperforms HUW balancing by 6.78% (MAE) and 3.50% (RMSE), and DWA by 6.60% (MAE) and 3.91% (RMSE). Furthermore, our approach further offers an additional 6.62% MAE and 3.86% RMSE improvement compared to EqW on both QoS parameters. This shows that the EMA-based strategy adapts quickly to task fluctuations, stabilizes task weighting, thereby mitigating negative transfer, and ensures balanced optimization, making it a more reliable loss-balancing strategy for joint QoS prediction.

D. Module Ablation Study

Table VII presents the module-wise ablation on the WSDREAM-2T dataset (RT, TP). A clear performance decline is observed across all ablated variants, reinforcing the necessity of each component. The full framework, comprising shared representations and structural features, consistently delivers the best performance. Removing the Cross-SNR module results in a noticeable drop in average accuracy (2.70% on RT, 12.34% on TP), indicating that different QoS parameters exhibit informative patterns that benefit one another. Eliminating either the HHGNNs or SNR blocks also degrades performance, showing that these components supply complementary signals,

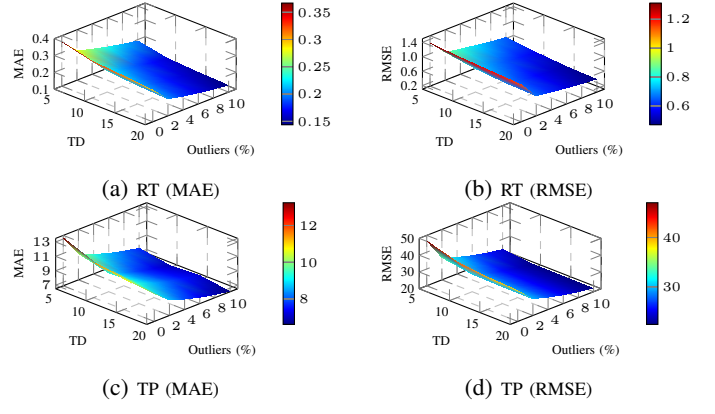


Fig. 4: Impact of outliers on WSDREAM-2T.

TABLE VIII: Impact of Cold-start on WSDREAM-2T

Training Density	QoS Para.	Type \downarrow CDF \downarrow	MAE				RMSE			
			0	5	10	20	0	5	10	20
10	RT	CB	0.3908	0.4304	0.5007		1.4103	1.5700	1.6888	
		CS	0.3243	0.3582	0.3783	0.4371	1.3330	1.4521	1.5392	
		CU	0.3666	0.3835	0.4000		1.3432	1.4223	1.4402	
	TP	CB	14.7406	18.6156	27.7954		51.1179	56.5571	77.0098	
		CS	11.4814	15.8290	16.2723	19.0722	41.7156	53.2600	54.8492	62.8405
		CU	12.7160	12.9015	14.7178		46.1673	46.9849	51.3352	
20	RT	CB	0.3588	0.4073	0.4588		1.3151	1.4440	1.5427	
		CS	0.2930	0.3288	0.3515	0.4067	1.1516	1.2559	1.3253	1.4634
		CU	0.3399	0.3482	0.3658		1.2768	1.2966	1.3368	
	TP	CB	13.6560	17.0083	19.9448		49.6500	54.9375	62.6331	
		CS	10.4069	13.4201	14.4766	21.9069	38.7746	48.8123	49.5523	64.9157
		CU	11.9470	12.6056	13.1524		43.0584	45.5650	46.2888	

QoS features via HHGNNs capture fine-grained service behavior, while contextual cues using SNR alleviate the sparsity and cold-start problem. The highest degradation occurs when two modules are removed (HHGNNs+SNR, SNR+Cross-SNR or HHGNNs+Cross-SNR), where removing HHGNNs+SNR yields smaller average drops (4.17% RT and 25.27% TP). This highlights that all three modules contribute substantially to performance, and their joint integration achieves the most accurate joint QoS prediction.

E. Outlier Sensitivity Analysis

Outliers have a substantial impact on QoS prediction performance [4]. We explicitly handle outliers during both training and inference. Empirical inspection shows that the WSDREAM-2T dataset contains a considerable number of anomalous QoS values. Thus, during training, we adopt the L_1 (MAE) loss, which is inherently more robust to outliers than the L_2 (MSE) loss. Furthermore, to quantify the influence of outliers during inference, we identify a fixed percentage of outliers using the Isolation Forest [31] and evaluate model performance after removing them.

Fig. 4 reports the results when eliminating 2%–10% of outliers (in increments of 2%) across all four training densities (5, 10, 15, 20). Performance consistently improves as larger proportions of outliers are removed, with gains saturating around the 8%–10% range. At 10% removal, SHARP-QoS achieves an average improvement of 81.84% compared to the setting where outliers are not addressed.

F. Cold-start Sensitivity Analysis

Cold-start represents new users or services that lack historical QoS records. QoS prediction methods that rely mainly on QoS-specific features often struggle in such situations.

TABLE IX: Use of different graphs on WSDREAM-2T

QoS Para.	Model	MAE		RMSE	
		10	20	10	20
RT	QoS	0.3318	0.3108	1.2598	1.2105
	QoS + AS	0.3299	0.3035	1.2605	1.1898
	QoS + RG	0.3290	0.3000	1.2592	1.1885
	Single Graph	0.3262	0.3003	1.2516	1.1852
TP	Ours	0.3243	0.2930	1.2450	1.1516
	QoS	12.7465	11.7712	48.0036	42.3711
	QoS + AS	12.1578	11.7534	45.5000	42.9646
	QoS + RG	12.0947	11.4153	43.0615	41.9777
	Single Graph	11.8777	11.3378	43.3086	41.3478
Ours	11.4814	10.4069	41.7156	38.7746	

SHARP-QoS incorporates public contextual attributes, including AS and region information, to deal with this.

To assess the sensitivity of our model to cold-start cases, we create three scenarios by randomly selecting a fixed percentage (CSP) of users and services and removing all their corresponding invocation entries from the QoS matrices: (i) *Cold-start User (CU)*: A fixed CSP of users is selected, and all their QoS entries are removed. (ii) *Cold-start Service (CS)*: A fixed CSP of services is selected, and all their QoS entries are removed. (iii) *Cold-start Both (CB)*: A fixed CSP of both users and services is selected, and all their corresponding entries are removed. All other data remain unchanged.

Table VIII presents the model performance under two training densities (10, 20) for WSDREAM-2T (RT, TP) dataset. The main observations are as follows: (i) As CSP increases (0-20, with a step-size of 5), performance declines for both RT and TP due to the reduction in available training data. (ii) For a fixed CSP, higher training density leads to better performance. (iii) Under the same CSP, the CB scenario shows the largest performance drop because more entries are removed compared to CU and CS.

These results show that SHARP-QoS demonstrates reasonable robustness in handling cold-start cases.

G. Impact of Context Graphs

Table IX evaluates the contribution of complementary contextual signals derived from AS and RG graphs. When HHGCNs are applied only to the QoS invocation graphs, the average performance drops by 3.51% in RT and 10.78% in TP relative to the full model performance, indicating that only QoS-based structural features are insufficient alone to achieve the best performance. Introducing either the AS or RG context graph improves performance, with the RG graph providing a stronger gain. This is likely due to the RG graph containing approximately $4.37 \times$ more edges, thereby offering richer collaborative cues. Furthermore, collapsing all edges into a single merged graph (a unified adjacency matrix) results in inferior performance compared to our design, which processes the QoS, AS, and RG graphs separately using HHGCN and HyGCN modules. The merged graph combines heterogeneous structural signals into a single message-passing process, potentially amplifying noise and weakening fine-grained feature propagation. In contrast, treating the context graphs independently exploits their complementary roles: the RG graph captures coarse geographical proximity, while the AS graph encodes fine-grained routing and peering relation-

TABLE X: Confidence Intervals on WSDREAM-2T.

Conf. level	RT-10	RT-20	TP-10	TP-20
90%	(0.2856, 0.3629)	(0.2699, 0.3293)	(10.9175, 11.9258)	(9.9840, 10.9102)
95%	(0.2782, 0.3703)	(0.2643, 0.3350)	(10.8210, 12.0224)	(9.8954, 10.9988)
99%	(0.2638, 0.3847)	(0.2531, 0.3461)	(10.6322, 12.2112)	(9.7219, 11.1722)
MAE \pm Std	0.3243 \pm 0.1773	0.2996 \pm 0.1362	11.4217 \pm 2.3139	10.4471 \pm 2.1253

Conf.: Confidence, Std: Standard deviation

ships. This isolated yet complementary modeling yields the optimal performance.

Hyperparameter sensitivity analysis is provided in Appendix B of the supp. file.

H. Statistical Significance Analysis

To ensure the reliability of SHARP-QoS, we perform a statistical significance analysis [32]. Specifically, we partition the test prediction errors into $G = 50$ equally sized, non-overlapping groups and compute the MAE of each group independently. Using these group-wise errors, we estimate the empirical mean \bar{m} and standard deviation s . We then compute the two-sided confidence intervals (CI) using Eq. 26 for confidence levels $\alpha \in \{90\%, 95\%, 99\%\}$ with their corresponding z -scores z_α , and present the results in Table X.

$$\text{CI}_\alpha = \left[\bar{m} - z_\alpha \frac{s}{\sqrt{G}}, \bar{m} + z_\alpha \frac{s}{\sqrt{G}} \right] \quad (26)$$

Hypothesis Validation: We assess stability by verifying whether the observed MAE falls within the confidence bounds $H_0 : \text{MAE}_{\text{obs}} \in \text{CI}_\alpha$. If satisfied, H_0 is accepted, indicating reliable performance; otherwise, it is rejected, suggesting potential instability or bias.

As shown in Table X, the observed MAE values (last row) for both RT and TP consistently fall within the computed confidence intervals across all confidence levels. Moreover, the confidence intervals narrow with increasing data density, indicating lower variance and improved reliability, thereby demonstrating that the prediction behavior across subgroups is statistically sound.

VI. RELATED WORK

This section reviews CF-based methods, covering both single-task and multi-task QoS prediction.

A. Single-task QoS Prediction Approaches

Traditional methods often utilize the prediction of a single QoS parameter. These approaches are categorized into three categories: memory-based, model-based, and hybrids. (i) **Memory-based methods** relied on statistical similarity measures (e.g. PCC, Cosine) among users/services. Prior methods, UPCC [6] used user-based, IPCC [7] adopted service-based, and WSRec [3] used combined similarity among both entities. While these methods are trivial, they are computationally complex and face standard challenges such as data sparsity, cold-start, scalability, and inability to extract higher-order features. (ii) **Model-based methods**, on the other hand, focus on learning latent user/service features by building predictive models. NMF [27] and PMF [8], used non-negative and probabilistic matrix factorization (MF), respectively, lacking in incorporating contextual attributes. Building on this, CSMF [33]

and GeoMF [34] proposed context-sensitive MF, which often raises privacy concerns due to the use of user/service private information, and face challenges due to outlier issues. CMF [4] enhances robustness via Cauchy loss, an outlier-resilient loss function, but fails to exploit nonlinear and higher-order features. To enhance expressivity, EFMPred [9] leverages up to second-order features via a factorization machine (FM). NDMF [35] and MM-DNN [10] exploit the higher-order features by combining MF with building a Multi-layer perceptron (MLPs). DCLG [36] integrate both linear correlations via dot-product and nonlinear higher-order relationships via MLP. IImQoS [12] enhances discrete text-based features using a language model (LM). The structure-based features are introduced by QoSGNN [11] using an attention-based MF framework over the service invocation graphs. *(iii) Hybrid Methods:* To further enhance the performance, recent methods combine both approaches. OffDQ [13] used QoS-based similarity features with deep architectures, NCRL [5] combined the context features and historical similarity via a two-tower deep residual network, and ARRQP [14] introduced an anomaly-resilient framework via QoS-based correlations and multi-head GCNs, achieving high single-task performance.

Collectively, these approaches excel in single QoS parameter prediction, ensuring high performance. However, when it comes to service optimality across multiple QoS parameters, these methods require that many similar models be trained, which leads them to increases in computational cost, and suffer from poor generalization due to under-utilization of shared information across QoS parameters.

B. Joint QoS Prediction Approaches

Recent research shows the evolving need for joint QoS prediction, which aims to simultaneously predict multiple QoS attributes using a unified framework. DNM [15] employed a deep architecture, leveraging additive and multiplicative inter-context feature interactions. JQSP [18] utilized ID-based features while leveraging GCNs with attention mechanisms. MGEN [19] used a mixture-of-experts architecture with location-based features, exploiting explicit shared information. HTG [20] used GATs focused on cold-start prediction. These methods often suffer from joint optimization due to the difference in numerical range of QoS parameters, leading to the negative transfer problem, which causes performance drop for some parameters while improving others. To address these disparities, PMT [16] employed a heteroscedastic uncertainty-based loss weighting mechanism, which balances the training using a multi-expert architecture via inner and Hadamard products, followed by an attention module. WAMTL [21] introduced an adaptive loss balancing approach via dynamic weight averaging (DWA), and leveraged a multi-gate mixture-of-experts framework.

Although these methods advance the joint QoS modeling but they still have key limitations: (i) Over-reliance on ID-based or topology-sensitive features compromises the scalability and privacy of users and services, (ii) Lack of modeling hierarchical dependencies among QoS parameters and global context factors, and (iii) Task dominance due to varying numerical

scale causing negative transfer during joint optimization, resulting in skewed results.

C. Positioning of Our Work

We propose SHARP-QoS, which integrates non-negative MF-based QoS features with contextual information derived from AS and region, ensuring domain-aware and privacy-preserving initial representations. To capture the implicit hierarchical features across both QoS and contextual domains, we employ hyperbolic convolutional networks (HyHCN and HHGCN). Leveraging subnetwork routing (SNR, Cross-SNR), the framework enables adaptive feature sharing for QoS and contextual features, followed by a gated fusion module that dynamically selects between hierarchical QoS representations and shared features. To ensure reliable joint learning, we incorporate a robust loss function with an EMA-based loss balancing strategy to mitigate negative transfer. Collectively, the proposed framework substantially enhances joint QoS prediction performance while remaining scalable, sparsity-tolerant, and resilient to noise.

VII. CONCLUSION

This paper proposes a unified framework for joint QoS prediction called SHARP-QoS that leverages hierarchical features via hyperbolic convolution networks, adaptive multi-context routing using QoS and contextual features, and an EMA-based loss balancing strategy. This enables higher-order, complex features while allowing for flexible feature sharing across QoS parameters, and effectively mitigating negative transfer and enhancing graph representation learning. Experimental results show that our method achieves superior prediction accuracy and inference latency compared to existing approaches. Future work will explore real-time service environments, deployment on resource-constrained devices, and integration of online measurement signals for dynamic graph updates.

REFERENCES

- [1] Z. Zheng *et al.*, “Web service QoS prediction via collaborative filtering: A survey,” *IEEE TSC*, vol. 15, no. 4, pp. 2455–2472, 2022.
- [2] S. H. Ghafouri *et al.*, “A survey on web service QoS prediction methods,” *IEEE TSC*, vol. 15, no. 4, pp. 2439–2454, 2022.
- [3] Z. Zheng *et al.*, “QoS-aware web service recommendation by collaborative filtering,” *IEEE TSC*, vol. 4, no. 2, pp. 140–152, 2011.
- [4] F. Ye *et al.*, “Outlier-resilient web service QoS prediction,” in *WWW*, 2021, pp. 3099–3110.
- [5] G. Zou *et al.*, “NCRL: Neighborhood-Based Collaborative Residual Learning for Adaptive QoS Prediction,” *IEEE TSC*, vol. 16, no. 3, pp. 2030–2043, 2023.
- [6] J. S. Breese *et al.*, “Empirical Analysis of Predictive Algorithms for Collaborative Filtering,” in *UAI*, 1998, pp. 43–52.
- [7] B. M. Sarwar *et al.*, “Item-based collaborative filtering recommendation algorithms,” in *WWW*, 2001, pp. 285–295.
- [8] R. Salakhutdinov and A. Mnih, “Probabilistic Matrix Factorization,” in *NIPS*, 2007, p. 1257–1264.
- [9] Y. Wu *et al.*, “An Embedding Based Factorization Machine Approach for Web Service QoS Prediction,” in *ICSO*, 2017, pp. 272–286.
- [10] P. Zhang *et al.*, “A Novel Deep-Learning-Based QoS Prediction Model for Service Recommendation Utilizing Multi-Stage Multi-Scale Feature Fusion With Individual Evaluations,” *IEEE TASE*, vol. 21, no. 2, pp. 1740–1753, 2024.
- [11] M. Liu *et al.*, “QoSGNN: Boosting QoS Prediction Performance With Graph Neural Networks,” *IEEE TSC*, vol. 17, no. 02, pp. 645–658, mar 2024.

- [12] H. Liu *et al.*, “Large language model aided qos prediction for service recommendation,” in *2025 IEEE ICSSE*. IEEE, 2025, pp. 116–127.
- [13] S. Chattopadhyay *et al.*, “OffDQ: An Offline Deep Learning Framework for QoS Prediction,” in *WWW*, 2022, p. 1987–1996.
- [14] S. Kumar and S. Chattopadhyay, “ARRQP: Anomaly Resilient Real-Time QoS Prediction Framework With Graph Convolution,” *IEEE TSC*, vol. 18, no. 3, pp. 1245–1261, 2025.
- [15] H. Wu *et al.*, “Multiple Attributes QoS Prediction via Deep Neural Model with Contexts,” *IEEE TSC*, vol. 14, no. 4, pp. 1084–1096, 2021.
- [16] H. Lian *et al.*, “Toward Effective Personalized Service QoS Prediction From the Perspective of Multi-Task Learning,” *IEEE TNSM*, vol. 20, no. 3, pp. 2587–2597, 2023.
- [17] R. Caruana, “Multitask learning,” *Machine learning*, vol. 28, no. 1, pp. 41–75, 1997.
- [18] L. Ding *et al.*, “Joint QoS Prediction for Web Services based on Deep Fusion of Features,” *IEEE TNSM*, pp. 1–1, 2023.
- [19] H. Luo, “Gated multi-task learning for qos-aware service recommendation,” in *Journal of Physics: Conference Series*, vol. 2547, no. 1. IOP Publishing, 2023, p. 012011.
- [20] M. Chen *et al.*, “HTG: A heterogeneous topology aware model to improve cold start in cloud service QoS prediction,” *Trans. Emerg. Telecommun. Technol.*, vol. 35, no. 3, Mar. 2024.
- [21] J. Wang *et al.*, “QoS Prediction Method via Multi-Task Learning for Web Service Recommendation,” in *2024 IEEE ICWS*, 2024, pp. 1353–1355.
- [22] J. Ma *et al.*, “SNR: sub-network routing for flexible parameter sharing in multi-task learning,” ser. AAAI’19/IAAI’19/EAII’19. AAAI Press, 2019.
- [23] Z. Zheng *et al.*, “Investigating QoS of Real-World Web Services,” *IEEE TSC*, vol. 7, no. 1, pp. 32–39, 2014.
- [24] O.-E. Ganea *et al.*, “Hyperbolic neural networks,” in *Proceedings of the 32nd NeurIPS*, ser. NIPS’18. Red Hook, NY, USA: Curran Associates Inc., 2018, p. 5350–5360.
- [25] I. Chami *et al.*, “Hyperbolic Graph Convolutional Neural Networks,” in *NeurIPS 2019, December 8-14, 2019, Vancouver, BC, Canada*, 2019, pp. 4869–4880.
- [26] T. N. Kipf and M. Welling, “Semi-Supervised Classification with Graph Convolutional Networks,” in *ICLR 2017, Toulon, France, April 24-26*, 2017.
- [27] D. D. Lee *et al.*, “Learning the Parts of Objects by Non-Negative Matrix Factorization,” *Nature*, vol. 401, no. 6755, p. 788, 1999.
- [28] P. Vincent *et al.*, “Stacked Denoising Autoencoders: Learning Useful Representations in a Deep Network with a Local Denoising Criterion,” *JMLR*, vol. 11, p. 3371–3408, dec 2010.
- [29] C. Louizos, M. Welling, and D. P. Kingma, “Learning Sparse Neural Networks through L_0 Regularization,” in *ICLR*, 2018.
- [30] D. Wu *et al.*, “A Data-Characteristic-Aware Latent Factor Model for Web Services QoS Prediction,” *IEEE TKDE*, vol. 34, no. 6, pp. 2525–2538, 2022.
- [31] F. T. Liu *et al.*, “Isolation forest,” in *IEEE ICDM*, 2008, pp. 413–422.
- [32] J. Demšar, “Statistical Comparisons of Classifiers over Multiple Data Sets,” *JMLR*, vol. 7, no. 1, pp. 1–30, 2006.
- [33] H. Wu *et al.*, “Collaborative QoS prediction with context-sensitive matrix factorization,” *FGCS*, vol. 82, pp. 669–678, 2018.
- [34] Z. Chen *et al.*, “Your neighbors alleviate cold-start: On geographical neighborhood influence to collaborative web service QoS prediction,” *Knowl. Based Syst.*, vol. 138, pp. 188–201, 2017.
- [35] G. Zou *et al.*, “NDMF: neighborhood-integrated deep matrix factorization for service QoS prediction,” *IEEE TNSM*, vol. 17, no. 4, pp. 2717–2730, 2020.
- [36] Z. Jia *et al.*, “Location-Aware Web Service QoS Prediction via Deep Collaborative Filtering,” *IEEE TCSS*, vol. 10, no. 6, pp. 3524–3535, 2023.

SUPPLEMENTARY APPENDIX

Appendices A and B are provided in <https://github.com/csksuraj17/SHARP-QoS>